Dependence of aggregation behavior on concentration in triblock copolymer solutions: The effect of chain architecture

Xiang-Gang Han and Xue-Feng Zhang

Citation: The Journal of Chemical Physics **143**, 214904 (2015); doi: 10.1063/1.4936581
View online: http://dx.doi.org/10.1063/1.4936581
View Table of Contents: http://scitation.aip.org/content/aip/journal/jcp/143/21?ver=pdfcov
Published by the AIP Publishing

Dependence of aggregation behavior on concentration in triblock copolymer solutions: The effect of chain architecture

Xiang-Gang Han[a] and Xue-Feng Zhang
Key Laboratory of Integrated Exploitation of Bayan Obo Multi-Metal Resources School of Mathematics, Physics and Biological Engineering, Inner Mongolia University of Science and Technology, Baotou 014010, China

(Received 28 July 2015; accepted 11 November 2015; published online 2 December 2015)

Using the self-consistent field lattice technique, the effects of concentration and hydrophobic middle block length (where the chain length remains constant) on aggregation behavior are studied in amphiphilic symmetric triblock copolymer solutions. The heat capacity peak for the unimer-micelle transition and the distribution peaks for the different degrees of aggregation for micelles and small aggregates (submicelles) are calculated. Analysis of the conducted computer simulations shows that the transition broadness dependence on concentration is determined by the hydrophobic middle block length, and this dependence is distinctly different when the length of the hydrophobic middle block changes. Different size for small aggregates simultaneously appear in the transition region. As temperature decreases, the number of different size small aggregates for the large hydrophobic middle block length first ascends and then descends in aggregation degree order. These results indicate that any transition broadness change with concentration is related to the mechanism of fragmentation and fusion. These results are helpful for interpreting the aggregation process of amphiphilic copolymers at equilibrium. © *2015 AIP Publishing LLC.* [http://dx.doi.org/10.1063/1.4936581]

I. INTRODUCTION

Amphiphilic block copolymers have been the subject of great interest in recent decades for their ability to self-assemble into micelles in a selective solvent. When the polymers contain only two distinct A and B chains (i.e., an AB diblock copolymer), micelles can form with A blocks in the core surrounded by a corona of B blocks. Adding an additional A block potentially increases the structural and dynamic complexity of the micelles.[1] In the simplest cases involving symmetric triblocks, BAB polymers may form hairy micelles with A blocks looped within the core. Block polymer micelles offer a host of applications, including drug delivery[2,3] viscosity modification[4,5] and colloidal and polymer blend stabilization.[6,7]

The micellization kinetics of block copolymer solutions have been an area of active study during the past decade. This interest is due to the fundamental importance of micellization kinetics in understanding polymer self-assembly and various industrial applications. Related studies have predicted various growth mechanisms. Some results favor the classical Aniansson-Wall mechanism,[8] an exchange of single molecules (unimers),[9–12] while others emphasize the role of fragmentation or recombination mechanisms.[13,14] Recently, Rharbi reported on the fusion and fragmentation that occurs at equilibrium in block copolymers.[15]

In amphiphilic block copolymers, there is an equilibrium region of the unimer-micelle transition above the critical micelle temperature. Various techniques have been used to detect this region, which is characterized by rapid changes in such variables as hydrophobicity, partial specific volume, heat capacity, and so on. Related studies demonstrated that the shapes and widths of the micellization peaks in amphiphilic block copolymers are influenced by the distribution of hydrophobic blocks lengths.[16,17] The broad nature of the unimer-micelle transition region (i.e., the equilibrium region of transition) may be ascribed to the structural changes which accompany the replacement of micellar core hydrophilic components with hydrophobic components.[18,19] Thus, the broadness of the transition should be interpreted using equilibrium kinetics. However, the actual mechanism behind the chain architecture effect on transition broadness has not been clarified.

Computer simulations have been a valuable tool for studying the phase behavior of polymers. All-atomic molecular dynamic (MD) simulations accurately address hydrodynamic interactions,[20–22] while permitting modeling of morphological evolution in polymeric systems during phase separation. Mesoscopic simulation methods also provide promising and widely accepted simulation approaches. Dissipative particle dynamics allows simulations on mesoscopic space and time scales, and the approach has been successfully used to model the thermodynamics and kinetics of surfactant and block copolymer micelle self-assembly.[23–26] In addition, self-consistent field theory (SCFT) is capable of capturing the essential characteristics of the self-assembly of copolymers in dilute solutions.[10,27–31] With the assistance of the real-space method proposed by Fredrickson,[32] Liang and co-workers investigated the aggregation behavior of amphiphilic diblock copolymers in selective solvents.[27,28]

In our previous works, we have used the SCFT lattice model to study the gelation of physically associating polymer solutions[33–35] and aggregation behavior in amphiphilic ABA

[a]Author to whom correspondence should be addressed. Electronic mail: xghan0@163.com

symmetric triblock copolymer solutions.[19,36] In this paper, the transition broadness dependence on concentration $\bar{\phi}_P$ and middle hydrophobic block length N_{st} is studied in amphiphilic symmetric BAB triblock copolymer solutions. The heat capacity peak for the unimer-micelle transition and the distribution peak for different aggregation degree for aggregates are calculated. It is shown that the change in transition broadness with concentration is explained by the fragmentation and fusion between aggregates.

II. THEORY

This section briefly describes the SCFT lattice technique for an n_P amphiphilic symmetric BAB triblock copolymer system which is assumed to be incompressible. As Figure 1 shows, each block molecule consists of N_{st} sticker segments forming the hydrophobic middle A block and N_{ns} nonsticker segments forming each hydrophilic end B block, all distributed over a lattice. The chain length of the polymer N is $N_{st} + 2N_{ns}$. In addition to the polymer, n_h solvent molecules are placed on the vacant lattice sites. Polymer monomers and solvent molecules have the same size and each occupies one lattice site. The total number of lattice sites is $N_L = n_h + n_P N$. Nearest neighbor pairs of stickers have an attractive interaction $-\epsilon$ with $\epsilon > 0$, which is the only non-bonded interaction in the present system. An approximation of the attractive interaction energy[33] can be expressed as

$$\frac{U}{k_B T} = -\chi \sum_r \widehat{\phi}_{st}(r)\widehat{\phi}_{st}(r), \tag{1}$$

where χ is the Flory-Huggins interaction parameter in the solution and equals $\frac{z}{2k_B T}\epsilon$ where z is the coordination number of the lattice used, $\sum_r$ means the summation over all r the lattice sites, and $\widehat{\phi}_{st}(r) = \sum_j \sum_{s\in st} \delta_{r,r_{j,s}}$ is the volume fraction of stickers on site r, where j and s are the indexes of the chain and the monomer of a polymer, respectively. Note that $s \in st$ indicates that the sth monomer is a sticker monomer.

In this simulation, the SCFT for the amphiphilic triblock copolymer system is similar to that of the physically associating polymers.[33] The only difference between the two is due to the chain architecture reflected in the end segment distribution function shown below. The free energy in the canonical ensemble F[33] is defined as

$$\frac{F[\omega_+,\omega_-]}{k_B T} = \sum_r \left\{ \frac{1}{4\chi}\omega_-^2(r) - \omega_+(r) \right\} - n_P \ln Q_P[\omega_{st},\omega_{ns}] - n_h \ln Q_h[\omega_h], \tag{2}$$

where Q_P is the partition function of a noninteraction polymer chain subject to the fields $\omega_{st}(r) = \omega_+(r) - \omega_-(r)$ and $\omega_{ns}(r) = \omega_+(r)$, which act on the sticker and nonsticker segments, respectively. In addition, Q_h is the partition function of a solvent molecule subject to the field $\omega_h(r) = \omega_+(r)$, which is defined as $Q_h = \frac{1}{n_h}\sum_r \exp(-\omega_h(r))$. Minimizing the free energy function F with $\omega_-(r)$ and $\omega_+(r)$ leads to the following saddle point equations:

$$\omega_-(r) = 2\chi\phi_{st}(r), \tag{3}$$

$$\phi_{st}(r) + \phi_{ns}(r) + \phi_h(r) = 1, \tag{4}$$

where

$$\phi_{st}(r) = \frac{1}{N_L}\frac{1}{z}\frac{n_P}{Q_P}\sum_{s\in st}\sum_{\alpha_s}\frac{G^{\alpha_s}(r,s|1)G^{\alpha_s}(r,s|N)}{G(r,s)} \tag{5}$$

and

$$\phi_{ns}(r) = \frac{1}{N_L}\frac{1}{z}\frac{n_P}{Q_P}\sum_{s\in ns}\sum_{\alpha_s}\frac{G^{\alpha_s}(r,s|1)G^{\alpha_s}(r,s|N)}{G(r,s)} \tag{6}$$

are the average numbers of sticker and nonsticker segments at r, respectively, and $\phi_h(r) = \frac{1}{N_L}\frac{n_h}{Q_h}\exp\{-\omega_h(r)\}$ is the average number of solvent molecules at r. Furthermore, Q_P can be expressed as $Q_P = \frac{1}{N_L}\frac{1}{z}\sum_{r_N}\sum_{\alpha_N} G^{\alpha_N}(r,N|1)$, where r_N and α_N denote the position and orientation of the Nth segment of the chain, respectively, and $\sum_{r_N}\sum_{\alpha_N}$ means the summation over all possible positions and orientations of the Nth segment of the chain. Following the scheme developed by Leermakers and Scheutjens,[37] $G^{\alpha_s}(r,N|1)$ is evaluated from the following recursive relation:

$$G^{\alpha_s}(r,s|1) = G(r,s)\sum_{r'_{s-1}}\sum_{\alpha_{s-1}}\lambda_{r_s-r'_{s-1}}^{\alpha_s-\alpha_{s-1}}G^{\alpha_{s-1}}(r',s-1|1), \tag{7}$$

where $G(r,s)$ is the free segment weighting factor and is expressed as $G(r,s) = \begin{cases}\exp(-\omega_{st}(r_s)), & s\in st\\ \exp(-\omega_{ns}(r_s)), & s\in ns\end{cases}$, and $\sum_{r'_{s-1}}\sum_{\alpha_{s-1}}$ means the summation over all possible positions and orientations of the (s-1)th segment of the chain. Note that the initial condition is $G^{\alpha_1}(r,1|1) = G(r,1)$ for all values of α_1. The transfer matrix λ is used to describe the polymer chain, which depends only on the chain model used, and we assume that

$$\lambda_{r_s-r'_{s-1}}^{\alpha_s-\alpha_{s-1}} = \begin{cases}0 & \alpha_s = \alpha_{s-1}\\ 1/(z-1) & \text{otherwise}\end{cases}. \tag{8}$$

Here, r' denotes the nearest neighboring site of r. r_s and α_s denote the position and bond orientation of the sth segment of the copolymer, respectively. α can be any of the allowed bond orientations depending on the lattice model used. Given these values, $G^{\alpha_s}(r,s|1)$ describes one of the end segment distribution function of the sth segment of the chain. The other end segment distribution function $G^{\alpha_s}(r,s|N)$ is evaluated

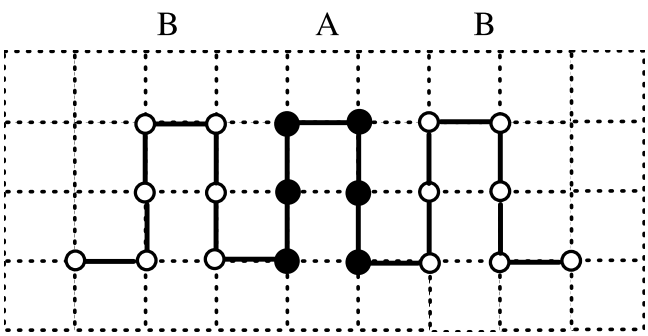

FIG. 1. Schematic of the triblock copolymer composed of sticker monomer segments (solid circles) and non-sticker monomer segments (open circles) distributed over a square lattice for $N_{st} = 6$.

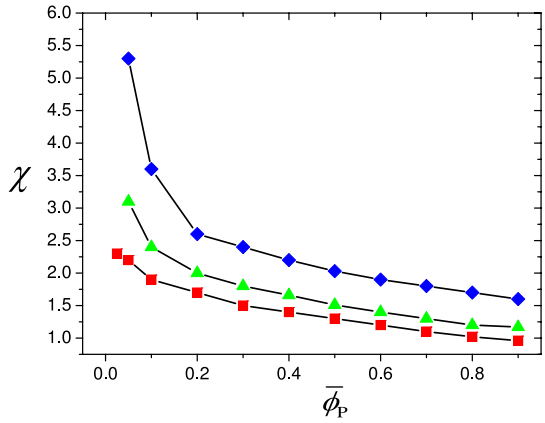

FIG. 2. The critical parameter for unimer-micelle transition χ_c for amphiphilic symmetric BAB triblock copolymers with different lengths of the hydrophobic middle block N_{st}. The red squares, green triangles, and blue diamonds correspond to the transition values when $N_{st} = 8$, 6, and 4, respectively.

from the following recursive relation:

$$G^{\alpha_s}(r,s|N) = G(r,s)\sum_{r'_{s+1}}\sum_{\alpha_{s+1}}\lambda^{\alpha_{s+1}-\alpha_s}_{r'_{s+1}-r_s}G^{\alpha_{s+1}}(r',s+1|N), \quad (9)$$

with the initial condition $G^{\alpha_N}(r,N|N) = G(r,N)$ for all the values of α_N. The value of λ indicates that the chain is described as a random walk without the possibility of direct backfolding. Although self-intersections of the chain are not permitted, the excluded volume effect is sufficiently taken into account.[38]

We use a pseudo-dynamic evolution process to calculate the saddle point,[33]

$$\omega_+^{new}(r) = \omega_+^{old}(r) + \lambda_+(\phi_{st}(r) + \phi_{ns}(r) + \phi_h(r) - 1), \quad (10)$$

$$\omega_-^{new}(r) = \omega_-^{old}(r) + \lambda_-(\phi_{st}(r) - \frac{\omega_-(r)}{2\chi}). \quad (11)$$

In our calculations, real space method is implemented to solve the SCFT equations in a cubic lattice with periodic boundary conditions. The calculation is initiated from appropriately randomly chosen fields $\omega_+(r)$ and $\omega_-(r)$, and stopped when the change of free energy F between two successive iterations is reduced to the needed precision. The resulting configuration is taken as a saddle point one. By comparing the free energies of the saddle point configurations obtained from different initial fields, the relative stability of the observed morphologies can be assessed.

III. RESULT AND DISCUSSION

In our study, the properties of symmetric BAB triblock copolymer solutions are characterized by four tunable parameters: χ (The Flory-Huggins interaction parameter), N (the chain length of the copolymer, which we maintained at

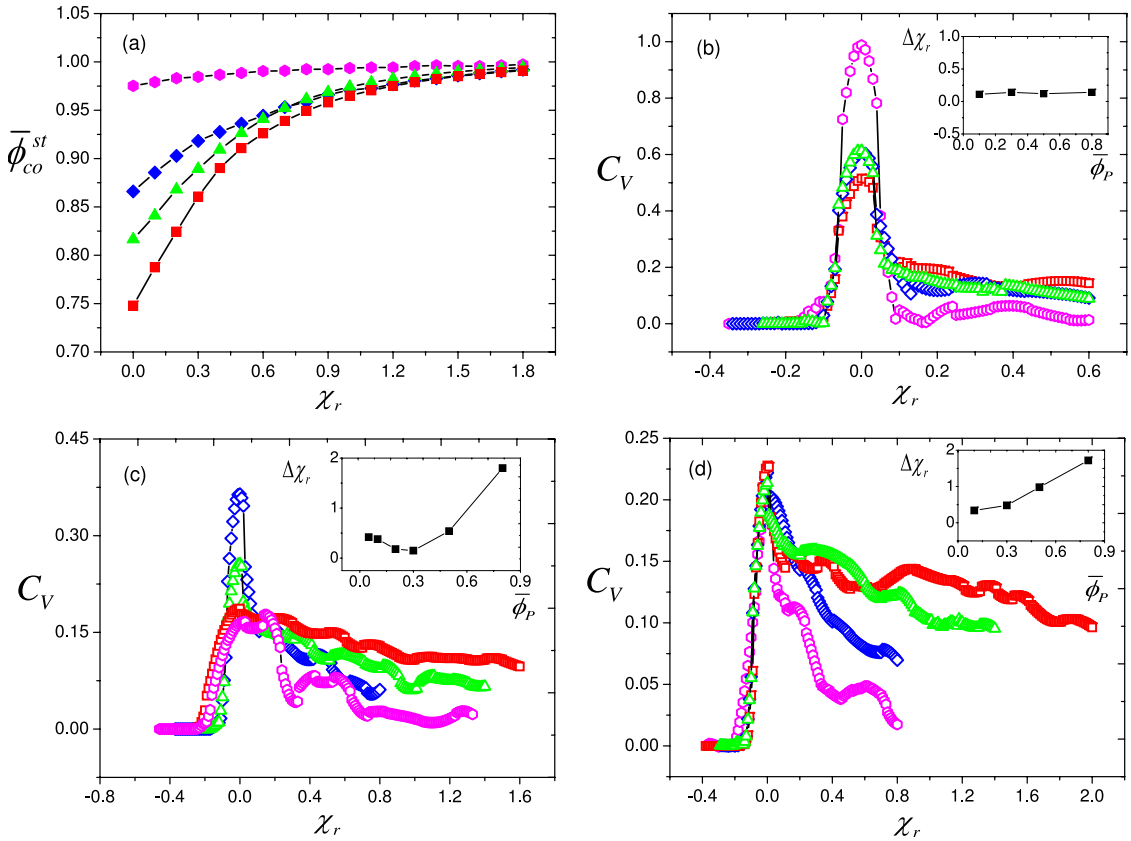

FIG. 3. (a) The variation of average volume fraction of stickers $\bar{\phi}^{st}_{co}$ at the micellar cores with χ_r $(=\chi-\chi_c)$ for various $\bar{\phi}_P$ when hydrophobic middle block lengths $N_{st} = 4$; (b) the change in heat capacity for (a); (c) the change in heat capacity when $N_{st} = 6$, and (d) the change in heat capacity when $N_{st} = 8$. The red squares, green triangles, blue diamonds, and magenta hexagons denote the cases of $\bar{\phi}_P = 0.8, 0.5, 0.3$, and 0.1, respectively. The inset in each image shows the change in half-width of the peak for the different values of $\bar{\phi}_P$.

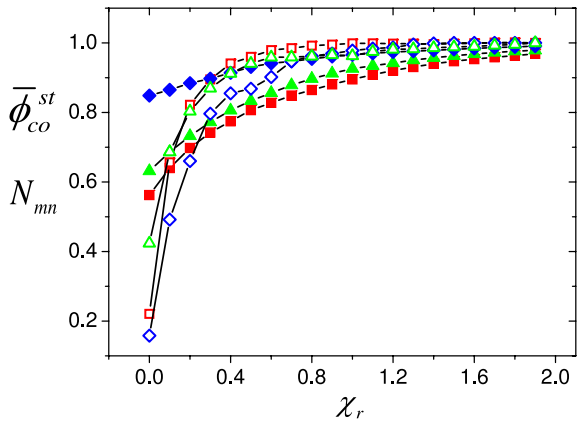

FIG. 4. Normalized (by its maximum) volume and average volume fraction of stickers for the micellar cores, denoted by N_{mn} and $\bar{\phi}_{co}^{st}$, respectively, as a function of different $\bar{\phi}_P$ values and a hydrophobic middle block length of $N_{st} = 8$. The red solid and open squares, green solid and open triangles, and blue solid and open diamonds correspond to $\bar{\phi}_P = 0.8, 0.5$, and 0.1, respectively. The solid points are $\bar{\phi}_{co}^{st}$ values and the hollow points are N_{mn} values.

$N = 20$), N_{st} (the length of the hydrophobic middle block), and $\bar{\phi}_P$ (polymer concentration). The results presented below are obtained from the lattice with $L = 26$. Fig. 2 shows the phase diagram of the systems with different hydrophobic middle block lengths. For any given value of N_{st}, a unimer-micelle transition occurs at χ_c if χ is increased sufficiently. When $\bar{\phi}_P$ is increased for a fixed N_{st}, the transition value χ_c descends. When N_{st} is decreased, and $\bar{\phi}_P$ remains fixed, χ_c ascends. Thus, increasing in polymer concentration and the length ratio of the hydrophobic to hydrophilic blocks creates a more favorable condition for unimer-micelle transition.

Above χ_c, micelles aggregate further as temperature decreases (i.e., an increase in χ). In order to clarify the temperature effect on aggregation, the change in average volume fraction of stickers at the micellar cores ($\phi_{co}^{st}(r) \geq 0.5$), $\bar{\phi}_{co}^{st}(r)$, with χ_r ($= \chi - \chi_c$) is calculated for various hydrophobic blocks lengths. Figure 3(a) shows that when $N_{st} = 4$ and $\bar{\phi}_P$ is fixed, $\bar{\phi}_{co}^{st}$ initially increases as χ_r increases, before eventually reaching a constant value. Note that $\bar{\phi}_{co}^{st}(r)$, for fixed χ_r, does not change monotonically with $\bar{\phi}_P$. For example, at intermediate concentrations, $\bar{\phi}_{co}^{st}(r)$ decreases as $\bar{\phi}_P$ increases when $\chi_r \leq 0.6$. When $N_{st} = 6$, the monotonic change in $\bar{\phi}_{co}^{st}$ as $\bar{\phi}_P$ changes occurs at $\chi_r = 0.4$, which is smaller than when $N_{st} = 4$. For the case of $N_{st} = 8$, however, $\bar{\phi}_{co}^{st}(r)$ with $\bar{\phi}_P$ changes monotonically for any fixed value of χ_r. It is shown that the effect of polymer concentration on micelles aggregation is dependent on the length of hydrophobic block for triblock copolymers.

The heat capacity may also be a characteristic of transition.[33,35,39] In this work, the heat capacity per site for amphiphilic symmetric BAB triblock copolymers is expressed as (in units of k_B)

$$C_V = \left(\frac{\partial U}{\partial T}\right)_{N_L, n_P} = \frac{1}{N_L}\chi^2 \frac{\partial}{\partial \chi}\left(\sum_r \phi_{st}^2(r)\right). \quad (12)$$

The $C_V(\chi_r)$ curve for the unimer-micelle transition for various $\bar{\phi}_P$ was calculated for different chain architectures. For $N_{st} = 4$ (Figure 3(b)) and $\bar{\phi}_P = 0.1$, the $C_V(\chi_r)$ curve exhibits a symmetrical peak. However, that peak symmetry decreases slightly at higher $\bar{\phi}_P$, while the half-width of peak, i.e., the transition broadness, remains constant. This result is in reasonable agreement with the experimental result observed by Liu *et al.*, who found that the variation of concentration in PEO-PPO-PEO block copolymer solutions, where the PPO block length ratio to chain length equals 0.26, does not influence the width of transition region.[40] When N_{st} is increased, the symmetry of the heat capacity peak clearly changes as $\bar{\phi}_P$ varies. In the case of $N_{st} = 6$ (Figure 3(c)), the symmetry of peak decreases with increasing $\bar{\phi}_P$, while the half-width of peak first decreases, and then increases again (inset of Figure 3(c)). Thus, the smallest value of the transition broadness appears at an intermediate concentration value of $\bar{\phi}_P \approx 0.3$. When $N_{st} = 8$ (Figure 3(d)), the half-width of peak increases linearly when $\bar{\phi}_P$ is increased. It is demonstrated that the effect of polymer concentration on transition broadness is remarkably dependent on hydrophobic block length. This dependence is in reasonable agreement with the above change in $\bar{\phi}_{co}^{st}(r)$ with concentration, which is also clearly relative to hydrophobic block length.

The unimer-micelle transition process can be subdivided three stages. The first stage is below the transition value χ_c. In the first stage, the copolymers exist in form of unimers. At χ_c micelles occur, indicating the start of the second stage. The micelles continue to aggregate as temperature decreases. As Figure 4 shows, given a fixed $\bar{\phi}_P$, the total micelle core volume and the average degree of micelle aggregation increase until reaching their respective plateau levels as temperature decreases. The occurrence of a constant value of the total micelle core volume means the end of the second stage, indicating the total micelle volume tends to be constant. In the third stage, the average degree of micelle aggregation changes with temperature, indicating the further adjustment of micelle aggregation. Although the unimer-micelle transition is an equilibrium transition, the three stages of the transition exist some similarity to the model of three stages of micellization proposed by Dormidontova *et al.*[13,26] They thought that during the first stage only small aggregates are formed, and no micelle forms, where the characteristic is similar to the first stage of the transition; at the second stage, micelles start to form and become dominant, which is consistent with the second stage for the transition. By the end of this stage, the total number of aggregates has equilibrated by the occurrence of the constant values for the number-average aggregation numbers; in the last stage, the main development of micellization process is redistribution of chains among micelles to achieve the equilibrium weight-average aggregation numbers distribution. This two quantities which characterize the last two stages of micellization are different from those characterize the ones of the above transition stages. If one considers the difference of characterization of number- and weight-average aggregation numbers for micelle aggregation, then the latter is more accurate than the former. This relative relationship is similar to the one of the average degree of micelle aggregation to the total micelle core volume. Thus, the relative characteristic of

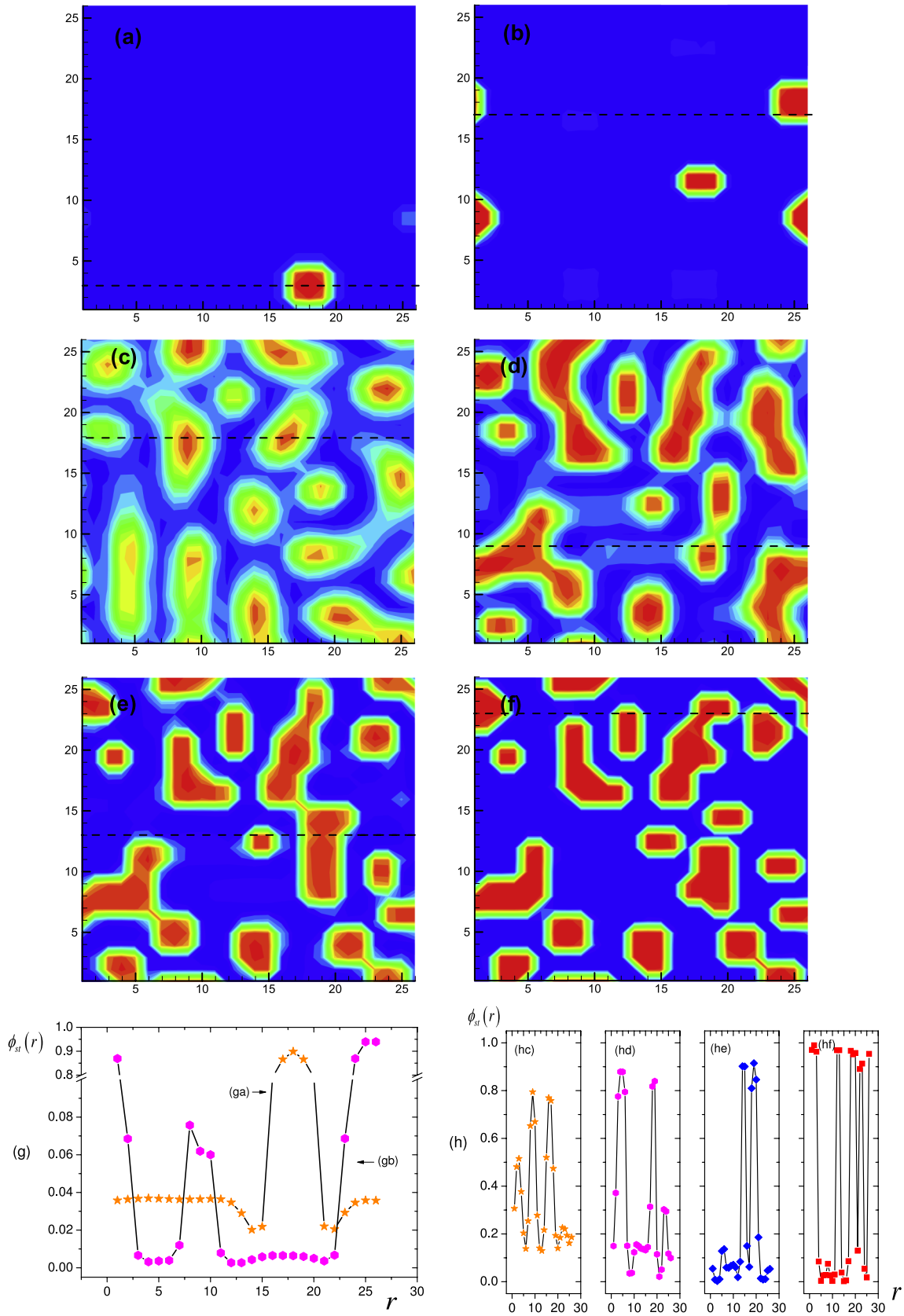

FIG. 5. Cross section of different concentration systems for $N_{st} = 8$. (a) and (b) show $\chi_r = 0.0$ and 0.4 for concentration of $\bar{\phi}_P = 0.1$, respectively; (c)–(f) corresponds to $\chi_r = 0.0$, 0.4, 0.8, and 1.6 for $\bar{\phi}_P = 0.8$, respectively; (g) and (h) the curve of $\phi_{st}(r)$ along a horizontal direction indicated by a dashed line in the above figure.

the last two stages of the transition stages is also similar to that of the last two stages of micellization.

As seen from Figure 4, the temperature dependence of the total micelle core volume increases as concentration decreases,

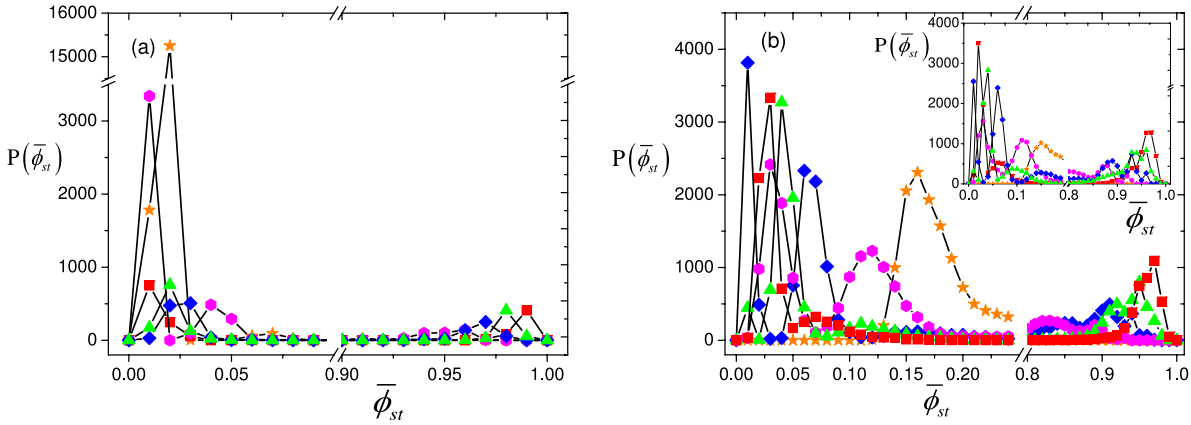

FIG. 6. Lattice site number distribution of the volume fraction of stickers for small aggregates and micelles (similar to distribution of the aggregation degree) with χ_r (=$\chi-\chi_c$), for various $\bar{\phi}_P$ at $N_{st}=6$. (a) $\bar{\phi}_P=0.1$; (b) $\bar{\phi}_P=0.8$, inset shows the same curves for $N_{st}=8$ and $\bar{\phi}_P=0.8$. The orange stars, magenta hexagons, blue diamonds, green triangles, and red squares denote the cases of $\chi_r=0.0$, 0.4, 0.8, 1.2, and 1.6, respectively.

while the one of the average degree of micelle aggregation decreases. Consequently, the temperature range dominated by the second stage increases as the concentration decreases, while the one dominated by the third stage decreases. When $\bar{\phi}_P = 0.1$, a constant value for the average degree of micelle aggregation occurs sightly quicker than the total micelle core volume, indicating in the third stage is no adjustment of micelle aggregation, while Figures 5(a) and 5(b) also demonstrate that the transition broadness is dominated by the second stage. In high concentrations the transition broadness is first affected by the second stage [Figures 5(c) and 5(d)] and then by the third stage [Figures 5(e) and 5(f)]. For intermediate concentration, the effect of the second stage is limited over a large temperature range, while the third stage effect is determined by the number of sticker segments N_{st} of a chain. For example at $N_{st} = 6$, the change in transition broadness with respect to $\bar{\phi}_P$ is nonlinear, and the minimum appears at intermediate concentrations. When $N_{st} = 8$, the transition broadness with concentration increases at the same rate. This is because that the third stage effect appears in the lower concentrations when N_{st} is increased. When $N_{st} = 4$, the additional aggregation space available to the micelles is small, and the effect of concentration on the transition broadness is weak. Thus, the symmetry of the transition peak changes only slightly with concentration.

It is found that the appearance of large amounts of small aggregates evidently influences the aggregation mechanism verified by other studies.[41–43] In order to demonstrate the mechanism underlying the transition dependence on concentration, the lattice site number distributions of the volume fractions of stickers (similar to the distribution of the aggregation number) for small aggregates and micelles is calculated in various temperature for $N_{st} = 6$. At χ_c, as shown in Figure 6, numerous small aggregates appear in addition to the micelles. At low concentrations (Figure 6(a)) and χ_c, there are two kinds of different size small aggregates. The aggregation degree of the small size one of the two is low (the $\phi_{st}(r)$ for most of small aggregates equals 0.02), and they occur at nearly all the lattice sites (Figure 5(a)). As temperature decreases, the small aggregates fragment and fuse with small aggregates or with micelles. When temperature drops sufficiently the smaller size one of the two disappears early.

As concentration increases, the aggregation degree of the small aggregates appearing at χ_c increases. Seen from Figure 6(b), at high concentrations ($\bar{\phi}_P$= 0.8) and χ_c, only a distribution peak of aggregation degree for all aggregates appears, i.e, the difference of aggregation degree among different kinds of aggregates behaves continuously, which is markedly different with low and intermediate concentrations. As temperature decreases, the peak is fissions into several peaks of small aggregates and micelles. As the temperature continues to decrease, in fact, the number of peaks of small aggregates decreases in succession according to the magnitude of the order of aggregation degree, which is similar the case of low concentrations. At the same time, the behaviors of the small aggregates accompany the change in distribution of aggregation degree of micelles. As concentration increases, the successive disappearance of small aggregates in a certain order within a larger temperature range, and the fission of the distribution peak of aggregation degree at high concentration accelerate the further aggregation of the micelles.[44] The strong dependence of transition broadness on concentration also confirms micelle aggregation versus the mechanism of aggregate fragmentation/fusion.

As discussed above, at low concentrations, the transition broadness is dominated by the second stage of the transition. At intermediate and high concentrations, the transition broadness is affected by both the second and third stages of the transition. In the second stage, an increases in the micelle core volume and the average aggregation of micelles as temperature decreases result from the contribution of collective micelle (containing small aggregates) fusion/fission. Simultaneously, the fusion between small aggregates also leads to an abnormal increase in the total volume fraction of sticker of larger size one of the two small aggregates from $\chi_r = 0$ to $\chi_r = 0.4$ when $\bar{\phi}_P = 0.1$ (Figure 6(a)). The above fusions are similar to the second one of micellization. In the third stage, the contribution of the fusion between small aggregates and micelles declines clearly when the third stage carries forward. This behavior is different with the one of small aggregates in the third stage of micellization, where the exchange of small aggregates

between micelles remains at a comparable level in all the third stage.

IV. CONCLUSION AND SUMMARY

The aggregation behavior dependence on concentration $\bar{\phi}_P$ and middle hydrophobic block length N_{st} (assuming a constant chain length $N = 20$) was studied in amphiphilic symmetric BAB triblock copolymer solutions, using the self-consistent field lattice technique. It is found that the transition broadness dependence on concentration is determined by the value of N_{st}, with distinctly different values for different values of N_{st}. This change in transition broadness with concentration can be explained using the three-stage model of the transition. For large values of N_{st} and low concentrations, the transition broadness is dominated by the second stage, which is characterized by the increase in micelle core volume and the average aggregation degree of micelles with decreasing temperature. With increased concentration, the broadness is instead determined by the third stage, where the average micellar aggregation degree markedly increases with temperature over a larger range. Furthermore, our results showed that the increase in micelle core volume and the change in average aggregation degree for the micelles are a function of the fragmentation and fusion among different aggregates.

ACKNOWLEDGMENTS

This research is financially supported by the National Nature Science Foundations of China (Grant No. 21564011).

[1]Y. Y. Han, H. Z. Yu, H. B. Du, and W. Jiang, J. Am. Chem. Soc. **132**, 1144 (2010).
[2]G. Gaucher, M. Dufresne, V. P. Sant, N. Kang, D. Maysinger, and J. Leroux, J. Controlled Release **109**, 169 (2005).
[3]K. Kataoka, A. Harada, and Y. Nagasaki, Adv. Drug Delivery Rev. **47**, 113 (2001).
[4]M. Schouten, J. Dorrepaal, W. J. M. Stassen, W. A. H. M. Vlak, and K. Mortensen, Polymer **30**, 2038 (1989).
[5]W. Anderson, "Block copolymers as viscosity index improvers for lubrication Oils," U.S. patent 3763044A (2 October 1973).
[6]B. Hirzinger, M. Helmstedt, and J. Stejskal, Polymer **41**, 2883 (2000).
[7]F. L. Baines, S. Dionisio, N. C. Billingham, and S. P. Armes, Macromolecules **29**, 3096 (1996).
[8]E. A. G. Aniansson and S. N. Wall, J. Chem. Phys. **78**, 1024 (1974).
[9]I. A. Nyrkova and A. N. Semenov, Macromol. Theory Simul. **14**, 569 (2005).
[10]X. He and F. Schmid, Phys. Rev. Lett. **100**, 137802 (2008).
[11]A. Halperin and S. Alexander, Macromolecules **22**, 2403 (1989).
[12]J. C. Neu, J. A. Canizo, and L. L. Bonilla, Phys. Rev. E **66**, 061406 (2002).
[13]E. E. Dormidontova, Macromolecules **32**, 7630 (1999).
[14]R. Pool and P. G. Bolhuis, Phys. Rev. Lett. **97**, 018302 (2006).
[15]Y. Rharbi, Macromolecules **45**, 9823 (2012).
[16]P. Linse, Macromolecules **27**, 6404 (1994).
[17]W. Batsberg, S. Ndoni, C. Trandum, and S. Hvidt, Macromolecules **37**, 2965 (2004).
[18]I. Goldmints, F. K. V. Gottberg, K. A. Smith, and T. A. Hatton, Langmuir **13**, 3659 (1997).
[19]X. G. Han, Y. H. Ma, and S. L. Ouyang, Condens. Matter Phys. **16**, 33601 (2013).
[20]P. J. Hoogerbrugge and J. M. V. Koelman, Europhys. Lett. **19**, 155 (1992).
[21]R. D. Groot and P. B. Warren, J. Chem. Phys. **107**, 4423 (1997).
[22]C. L. Fu, Z. Y. Sun, and L. J. An, J. Phys. Chem. B **115**, 11345 (2011).
[23]A. Schlijper, P. Hoogerbrugge, and C. Manke, J. Rheol. **39**, 567 (1995).
[24]N. Spenley, Europhys. Lett. **49**, 534 (2000).
[25]W. Jiang, J. Huang, Y. Wang, and M. Laradji, J. Chem. Phys. **126**, 044901 (2007).
[26]Z. Li and E. E. Dormidontova, Macromolecules **43**, 3521 (2010).
[27]X. He, H. Liang, L. Huang, and C. Pan, J. Phys. Chem. B **108**, 1731 (2004).
[28]Y. Jiang, T. Chen, F. Ye, H. Liang, and A. C. Shi, Macromolecules **38**, 6710 (2005).
[29]L. Zhang, J. Lin, and S. Lin, J. Phys. Chem. B **111**, 9209 (2007).
[30]L. Zhang, J. Lin, and S. Lin, Macromolecules **40**, 5582 (2007).
[31]D. Duque, J. Chem. Phys. **119**, 5701 (2003).
[32]G. H. Fredrickson, *The Equilibrium Theory of Inhomogeneous Polymers* (Oxford University Press, Oxford, 2006).
[33]X. G. Han and C. X. Zhang, J. Chem. Phys. **132**, 164905 (2010).
[34]X. G. Han, X. F. Zhang, Y. H. Ma, C. X. Zhang, and Y. B. Guan, Condens. Matter Phys. **14**, 43601 (2011).
[35]X. G. Han, X. F. Zhang, and Y. H. Ma, Condens. Matter Phys. **15**, 33602 (2012).
[36]X. G. Han, Y. H. Ma, and S. L. Ouyang, Condens. Matter Phys. **17**, 23604 (2014).
[37]F. A. M. Leermakers and J. M. H. M. Scheutjens, J. Chem. Phys. **89**, 3264 (1988).
[38]Y. G. Medvedevskikh, Condens. Matter Phys. **4**, 209 (2001).
[39]J. F. Douglas, J. Dudowicz, and K. F. Freed, J. Chem. Phys. **125**, 114907 (2006).
[40]Y. L. Su, J. Wang, and H. Z. Liu, Macromolecules **35**, 6426 (2002).
[41]X. Liang, C. Guo, J. Ma, J. Wang, S. Chen, and H. Liu, J. Phys. Chem. B **111**, 13217 (2007).
[42]J. Y. Zhang, J. Xu, and S. Y. Liu, J. Phys. Chem. B **112**, 11284 (2008).
[43]J. Y. Rao, J. Y. Zhang, J. Xu, and S. Y. Liu, J. Colloid Interface Sci. **328**, 196 (2008).
[44]E. G. Kelley, R. P. Murphy, J. E. Seppala, T. P. Smart, S. D. Hann, M. O. Sullivan, and T. H. Epps, Nat. Commun. **5**, 3599 (2014).